Numerical ferromagnetic resonance experiments in nanosized elements

Wagner, K.; Körber, L.; Stienen, S.; Lindner, J.; Farle, M.; Kakay, A.;

Originally published:

January 2021

IEEE Magnetics Letters 12(2021), 6100205

DOI: https://doi.org/10.1109/LMAG.2021.3055447

Perma-Link to Publication Repository of HZDR:

https://www.hzdr.de/publications/Publ-31456

Numerical ferromagnetic resonance experiments in nano-sized elements

Kai Wagner[1,2], Lukas Körber[1,3,*], Sven Stienen[1,2], Jürgen Lindner[1], Michael Farle[2] and Attila Kákay[1]
[1]Helmholtz-Zentrum Dresden - Rossendorf, Institute of Ion Beam Physics and Materials Research, Bautzner Landstraße 400, 01328 Dresden, Germany
[2]Faculty of Physics and Center for Nanointegration (CeNIDE), University of Duisburg-Essen, Lotharstr. 1, 47057 Duisburg, Germany
[3]Fakultät Physik, Technische Universität Dresden, D-01062 Dresden, Germany
[*]Member, *IEEE*

We present a numerical approach to obtain the Ferromagnetic Resonance (FMR) spectra of micrometer- and nano-sized magnetic elements by micromagnetic simulations. Mimicking common experimental conditions, a static magnetic field is applied and a linearly polarized oscillating magnetic field is used to excite magnetization dynamics. A continuous single-frequency excitation is utilized, which permits to study the steady-state dynamics in space- and time-domain. This gives direct access to resonance fields, line widths and relative amplitudes as observed in the experiments, which is not easily accessible in pulsed schemes and allows for a one-to-one identification between simulation and experiment. Similar to numerical approaches using pulsed excitations the phases, ellipticity and spatial mode profiles of the spin-wave resonances (SWR) may also be accessed. Using large excitation powers we then showcase that one can additionally study nonlinear responses by this method such as the nonlinear shift of the resonance fields and the fold-over of the absorption lines. Since the dynamic susceptibility is directly determined from standard outputs of common micromagnetic codes, the presented method is robust, efficient and easy-to-use, adding to its practical importance.

Index Terms—**Ferromagnetic resonance, micromagnetic simulations, line width, nonlinear, fold-over**

I. Introduction

The detailed understanding of spin-wave resonances (SWR) of magnetic micro- and nanostructures and their magnetization dynamics has found increasing interest from both fundamental and application points of view for example in spin caloritronics and spin torque phenomena [1], [2], [3], [4], [5].

A powerful tool to measure spin-wave spectra with high spectral resolution is the Ferromagnetic Resonance (FMR), either detected directly in the frequency domain or in the field-swept mode at constant excitation frequency [6], [7]. In most cases the measured FMR-spectra are complex in nature, featuring several – often overlapping – resonances and require theoretical models of the nanostructured magnetic systems to extract quantitative information. Micromagnetic simulations of the FMR can be used to model such systems to provide information on the observed magnetic excitations, such as their character and dependence on magnetic parameters, geometries or charge currents [8], [9]. The micromagnetic approach is especially advantageous for complex geometries or interactions of nanoscale ferromagnets, when analytic approaches are not available.

Here, we present a numerical method to calculate the FMR of micrometer- and nano-sized magnetic elements by micromagnetic simulations. To closely mimic the experimental conditions of continuous-wave FMR detection, we use an alternative approach to the common field-pulse excitation scheme. In addition to a static magnetic field a single-frequency linearly-polarized oscillating magnetic field is used to excite magnetization dynamics. The observed SWR can be analyzed in the space- and time-domain. We show the relation between the volume averaged magnetization dynamics and the complex dynamic susceptibility tensor. With our approach one obtains not only information about the resonance fields, but also the otherwise difficult to obtain accurate line widths, relative intensities, ellipticity of the magnetization precession and phase relations of the excited SWR in the observed spectrum. These simulated parameters can be directly compared to the experimental data in a straightforward manner. The FMR spectra for large amplitude microwave fields with its usual characteristics as the nonlinear frequency shift of the resonance fields or the fold-over of the absorption curves can also be calculated, which is not accessible with the commonly-used field-pulse excitation method.

The spatially resolved magnetic response, plotted as a function of the external magnetic field and excitation frequency, yields a direct and detailed visualization of the SWR and their localization to different regions of the magnetic samples.

Corresponding author: K. Wagner (email: kai.wagner@unibas.ch, current address: Physics Department, University of Basel, Klingelbergstrasse 82. 4056 Basel, Switzerland)

II. Theoretical background

In the continuum limit, the dynamics of the magnetization $\boldsymbol{M}(\boldsymbol{r},t)$ in a ferromagnetic body is described by the Landau-Lifshitz-Gilbert equation: [10],

$$\frac{1}{\gamma}\frac{\mathrm{d}\boldsymbol{M}}{\mathrm{d}t} = -\left(\boldsymbol{M}\times\boldsymbol{H}_{\mathrm{eff}}\right) + \frac{\alpha}{M_{\mathrm{s}}}\left(\boldsymbol{M}\times\frac{\mathrm{d}\boldsymbol{M}}{\mathrm{d}t}\right) \qquad (1)$$

where $\boldsymbol{H}_{\mathrm{eff}}$ is the effective field comprising the exchange, dipolar, anisotropy and external magnetic fields, M_{s} is the saturation magnetization, γ is the gyromagnetic ratio of the

electron and α is the Gilbert-damping parameter. When the magnetization is deflected away from its equilibrium, *e.g.* by an external magnetic field, a precession around the effective field occurs. By separating the magnetization into a static and a dynamic part $\boldsymbol{M}(\boldsymbol{r},t) = \boldsymbol{M}_{\mathrm{eq}}(\boldsymbol{r}) + \boldsymbol{m}(\boldsymbol{r},t)$, one can linearize Eq. (1) with respect to small-amplitude excitations $\boldsymbol{m}(\boldsymbol{r},t)$. As a result, the high-frequency response of a magnetic system to an external microwave (RF) field $\tilde{\boldsymbol{h}}_{\mathrm{RF}}$ can be expressed using the Polder susceptibility tensor $\hat{\boldsymbol{\chi}}(\omega)$ as

$$\tilde{\boldsymbol{m}}(\boldsymbol{r},t) = \hat{\boldsymbol{\chi}}(\omega) \cdot \tilde{\boldsymbol{h}}_{\mathrm{RF}}(\boldsymbol{r},t) \tag{2}$$

Here, we use the complex-amplitude notation such that the real parts $\boldsymbol{m} = \Re(\tilde{\boldsymbol{m}})$ and $\boldsymbol{h}_{\mathrm{RF}} = \Re(\tilde{\boldsymbol{h}}_{\mathrm{RF}})$ correspond to the respective physical observables. The Polder tensor $\hat{\boldsymbol{\chi}}$, also referred to as dynamic susceptibility or high-frequency magnetic susceptibility, is a superposition of susceptibilities of the individual SWR and describes their linear response to the RF field, *i.e.* their resonance frequencies and line widths. The susceptibility may be split into a real and an imaginary part, $\hat{\boldsymbol{\chi}} = \hat{\boldsymbol{\chi}}' + i\hat{\boldsymbol{\chi}}''$. For a spatially homogeneous microwave field, the average power P absorbed by the magnetic system is proportional to the imaginary part of the Polder tensor [11],

$$P(\omega) \propto \langle \tilde{\boldsymbol{h}}^{*}_{\mathrm{RF}} \cdot \hat{\boldsymbol{\chi}}''(\omega) \cdot \tilde{\boldsymbol{h}}_{\mathrm{RF}} \rangle \tag{3}$$

Here, $\langle ... \rangle$ denotes the spatial average in the sample volume and the asterisk denotes the complex conjugate. As the signal measured in a conventional cavity-based FMR experiment is proportional to the average absorbed microwave power, simulating a FMR spectrum comes down to obtaining the imaginary part of the dynamic susceptibility $\hat{\boldsymbol{\chi}}''$. In typical FMR experiments, the frequency of the microwave field is kept constant and the static external field, hence the resonance frequencies, are varied. We may therefore consider the absorbed power as a function of static external field, $P(H)$.

III. Method

In micromagnetic simulations, which rely on numerically solving a discretized version of the equation of motion Eq. (1), the *modus operandi* to calculate the SWR susceptible to a microwave field with a certain spatial profile is a pulsed excitation scheme. A short magnetic field pulse of $\mathrm{sinc}(\omega_c t) = \sin(\omega_c t)/(\omega_c t)$ time dependence is applied followed by a Fourier transform of the magnetization dynamics. The latter can be done on the average magnetization components or individually on all discretization cells. Although this method allows to quickly obtain the linear resonance frequencies and spatial profiles of the excitable SWR below a certain cut-off frequency ω_c, it does not provide correct line widths, phases or relative amplitudes, as measured in FMR experiments. Moreover, the simultaneous and short-timed excitation of different Fourier components does not lead to steady-state dynamics and prohibits to study equilibrium nonlinear dynamics and related energy flow. The method presented here is free of these shortcomings.

Generally speaking, our approach is much better adapted to replicate the conditions of conventional FMR experiments. A homogeneous microwave field is applied and set to a fixed frequency and an additional static external field is slowly varied step-wise. For each field step, the microwave absorption is calculated based on Eq. (3), as will be explained in the following example. Whenever the field-dependent SWR frequencies match the frequency of the external microwave field, a local maximum in the power absorption, *i.e.* in the imaginary part of the dynamic susceptibility, is observed.

As an example, we consider a thin magnetic element, oriented in the xy-plane (see Fig. 1a). The static field is set to a chosen maximum value H_{max} and oriented along the x direction. The static equilibrium magnetization $\boldsymbol{M}_{\mathrm{eq}}$ is then found either by minimizing the torque given by Eq. (1) or by minimizing the total magnetic energy. To excite magnetization dynamics the direction of the spatially homogeneous linearly polarized microwave $\boldsymbol{h}_0 \sin(\omega t)$ at fixed angular frequency ω is chosen along the out-of-plane (z) direction. Following Eq. (3) the absorbed microwave power is in this case proportional to the imaginary part of the diagonal matrix element χ''_{zz}.

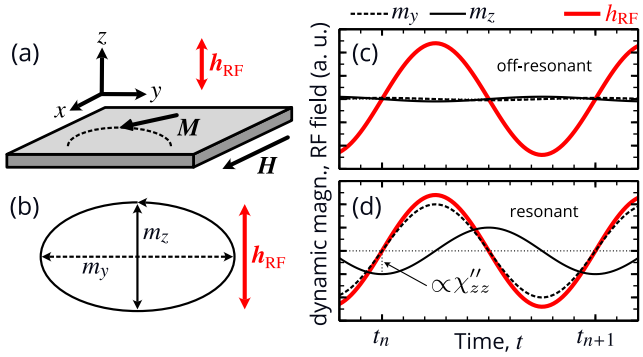

Fig. 1. The time dependent dynamic magnetization driven by an external RF field $\boldsymbol{h}_{\mathrm{RF}}$ for an infinite thin film magnetized in the xy-plane, as sketched in (a). The static field $\boldsymbol{H}$ is oriented in the film plane (x-direction) and is chosen to match the resonance condition. (b) The ellipticity of the SWR can be determined from the dynamic components of the magnetization. The normalized components (solid and dashed black lines) in the yz-plane are shown together with the amplitude of the RF field $\boldsymbol{h}_{\mathrm{RF}}$ (red line) along one period of excitation for the off-resonance (c) and resonance (d) cases. As marked in (d), the imaginary part of the susceptibility χ''_{zz} is proportional to the averaged out-of-plane component of the magnetization at the point when the RF field is crossing the zero value.

After an initial transient time, the torque exerted by the microwave field on the magnetization compensates the natural magnetic damping mechanisms and leads to stable oscillations in the dynamical components m_y and m_z at the angular frequency ω. Typically, in thin in-plane magnetized elements the magnetic precession trajectory is elliptical due to the dipolar interaction, as seen in Fig. 1b. To account for the initial transient phase, the magnetization is allowed to evolve for an integer number of time periods, $t_n = 2\pi \cdot n/\omega$, where n is chosen to provide a constant precession amplitude between consecutive oscillation cycles of the magnetization with a deviation of less than $0.02\,\%$. n typically depends on the magnetic parameters (*e.g.* damping constant α) and the micromagnetic solver at hand. Fig. 1c,d shows such a precession of the dynamical magnetization together with the RF field for the off-resonant and resonant cases. At resonance, the component parallel to the microwave field, m_z, has a phase

shift of $\pi/2$ with respect to the field, *i.e.* it has a local mininum when the field crosses zero at t_n. By inserting the sampling time t_n (periods of the RF field) into Eq. (2), taking the real part and averaging for the sample volume the microwave-absorption power reads as

$$P \propto \langle \chi''_{zz} \rangle = -\frac{\langle m_z(t_n) \rangle}{h_0} \tag{4}$$

with $h_0 = |\boldsymbol{h}_0|$ being the modulus of the RF amplitude. Hence, by monitoring the average dynamical component $\langle m_z \rangle$ parallel to the RF field $\boldsymbol{h}_{\mathrm{RF}}$ an absorption proportional to the FMR-signal can be obtained numerically, without further post processing. By a similar logic, the real part of the average susceptibility $\langle \chi'_{zz} \rangle$ - and therefore the complete $\langle \chi_{zz} \rangle$ - can be retrieved by extracting $\langle m_z \rangle$ at the maximum of the microwave field, *i.e.* at $t_{n+1/4}$. This makes the method extremely efficient and practical, especially since the averaged magnetization is provided by default by most micromagnetic codes.

The field-dependent absorption curve $P(H)$ is obtained by step-wise decreasing the static external field H and repeating the described procedure for each field step.

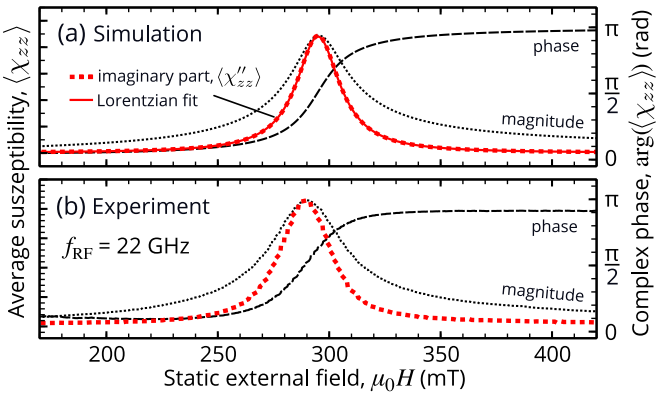

Fig. 2. (a) Micromagnetic simulation of the imaginary part, phase and magnitude of the average Polder susceptibility for an infinite thin film of 10 nm thickness. A microwave frequency of 22 GHz is applied, while the static magnetic field is swept step wise downwards. The material parameters are typical parameters for thin-film cobalt with $M_{\mathrm{s}} = 1230\,\mathrm{kA\,m^{-1}}$, $\gamma/2\pi = 29.8\,\mathrm{GHz\,T^{-1}}$ and a slightly increased damping $\alpha = 0.016$ to account for material inhomogeneities. The magnetic resonance exhibits the classical hallmarks of a driven oscillator, where the magnitude has positive skew with respect to the external field. The imaginary part is a Lorentzian curve proportional to the experimentally detected FMR signal shown in (b). The resonance field of the experiment is different to the simulation, since in the numerics the value of the saturation magnetization is only an effective value as obtained by fitting the well-known Kittel formula to the experimental data, neglecting crystal anisotropy [10].

As seen in Fig. 2a, the magnetic response (represented by the average matrix element $\langle \chi''_{zz} \rangle$), shows the typical hallmarks of a driven oscillator in respect to phase and magnitude. The imaginary part is a perfect Lorentzian absorption curve [22]. This allows to determine the resonance positions, their line width and relative signal strength. The results to an experimentally measured absorption curve for a 10 nm thick Co film in Fig. 2b, shows an excellent agreement with the simulation. The experimental curve was obtained using a coplanar waveguide (CPW)-FMR setup [16].

In case of multiple superimposed resonances a decomposition of the resultant spectra (experiment or simulation) into Lorentzian absorption lines is needed. The simulated spectra can be directly compared to complex experimental results as for example for the case of micrometer-sized magnetic stripes [14], [15], [18].

Next to these spectra, one may extract the spatial profile of the resonant SWR by considering the magnetization $\boldsymbol{M}(\boldsymbol{r}, t_n)$ of each cell. Moreover, in most cases, the average precession ellipticity is obtained by sampling the average dynamical components ($\langle m_{y,z} \rangle$) for a large number of points within an additional period $[t_n, t_{n+1}]$.

IV. Applications

To showcase this method we use a custom version of the GPU-accelerated micromagnetic code MuMax^3 [25], [26] which solves Eq. (1) on a cuboid grid. However, the method presented here is completely independent of the micromagnetic code at hand. Alternatives include OOMMF [12], TetraMag [27], NMAG-FinMag-Finimag [28] and LLG Micromagnetic Simulator [29], among others. Of course, this method could also be used for simple macro-spin simulations.

1) Characterizing the linear excitations in a magnetic element

As a first example, we characterize the magnetic excitations observable in FMR experiments in a $5.1\,\mu\mathrm{m} \times 1.1\,\mu\mathrm{m} \times 50\,\mathrm{nm}$ stripe made of permalloy ($Ni_{80}Fe_{20}$). For the material properties we adopt typical values of the exchange constant $A_{\mathrm{ex}} = 13\,\mathrm{pJ\,m^{-1}}$, saturation magnetization $M_{\mathrm{s}} = 790\,\mathrm{kA\,m^{-1}}$, reduced gyromagnetic ratio $\gamma/2\pi = 29.67\,\mathrm{GHz\,T^{-1}}$ and Gilbert-damping parameter $\alpha = 0.006$. To mimic experimental conditions, the static external field is slightly tilted in-plane by a $0.5°$ angle towards the short axis of the stripe. The number of periods n before sampling is set to 130. For codes based on double precision, *e.g.* OOMMF, this number can be smaller. The numerical microwave absorption together with the stripe geometry and field orientations are shown in Fig. 3a.

In such a confined system multiple SWR (in this case 3, labeled from 1 to 3) with differing resonance field positions, line widths and intensities occur [23]. The spatial distribution of the out-of-plane component of the dynamic magnetization, $m_z(t_n)$ is shown for the two most intense resonances in Fig. 3c,d. As discussed in Sec. III, these mode profiles are the natural outcomes of this continuous-wave excitation method. In Fig. 3b, we compare the numerical absorption curve to an experimental resonance line obtained from a real sample with the same dimensions and parameters, using a microresonator cavity. In contrast to the CPW-FMR technique, a single ferromagnetic object can be measured with a microresonator [14], [15], [17]. Since, experimentally, the microwave absorption was measured using a lock-in technique the derivative of both curves with respect to external field is shown. The experimental resonance fields are slightly different from the simulations which is likely due to fact that the saturation magnetization M_{s} and gyromagnetic ratio γ of the sample are not precisely known, as they were obtained from the FMR measurements. For better clarity, in Fig. 3b, we only show the simulation data for the resonances observed in the experiments.

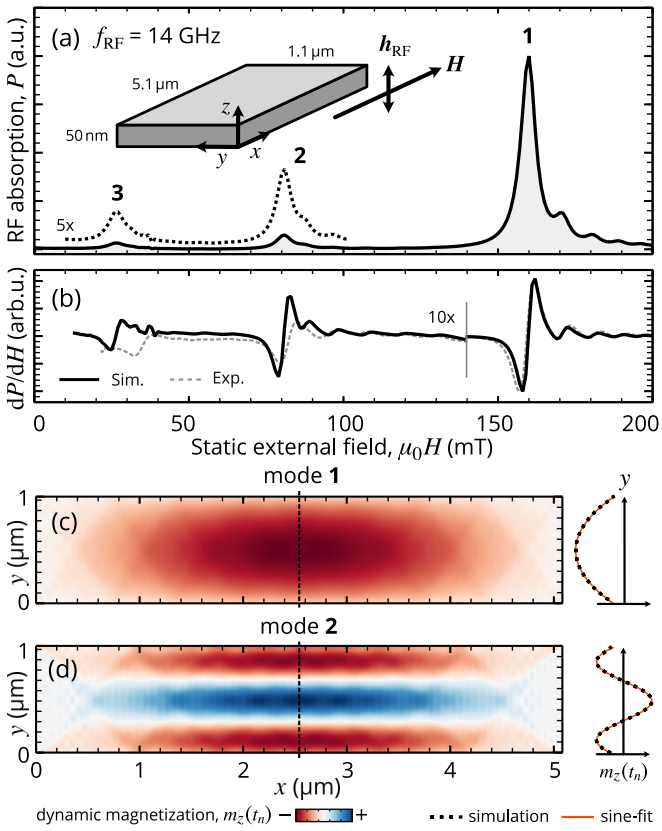

Fig. 3. (a) Micromagnetic simulation of the susceptibility χ''_{zz} for a $5.1\,\mu\mathrm{m}\times1.1\,\mu\mathrm{m}\times50\,\mathrm{nm}$ permalloy stripe and a fixed RF frequency of $14\,\mathrm{GHz}$. Multiple SWR are observed (labeled from 1 to 4). The derivative of the absorption curve is compared with an experimental curve in (b). The peaks are shifted probably due to a slightly different value of M_s in the simulations. For clarity, the simulation data is only shown for the experimentally observed resonances. (c,d) show the spatial profiles (out-of-plane component of the dynamic magnetization, m_z, at t_n) of the two lowest-order modes together with line scans of m_z taken the along the dashed lines.

In the numerical FMR spectra Fig. 3a the mode 1 is strongest in the center of the stripe and will here be referred to as a localized quasi-uniform mode. A different character can be observed for the less intense mode 2. Its out-of-plane component shows a change in sign across the stripe, two nodal lines and a wave-like varying dependence along the width of the stripe. Both modes can be very well approximated by a sinusoidal function as shown in Fig. 3c and d and resemble the expected mode profile of a standing SWR with wavelengths $2704\,\mathrm{nm}$ and $840\,\mathrm{nm}$ for the mode 1 and 2, respectively. These wavelengths differ from the expected values for simply closed or open pinning conditions and are a result of the dipolar pinning at the edges of the stripe [24]. The resonances 3 and 4 can be assigned to higher-order standing spin waves across the width of the stripe, with decreasing wavelengths for smaller resonance fields.

By such a spatial analysis one can for example explore the dependence of the microwave absorption spectra and magnetic excitations on the magnetic parameters as well as on the exact geometry of the magnetic systems. This information can be crucial for planning experiments and deeper understanding of the possibly large number of resonances in measured spectra, *e.g.* as also performed in [30]. This method can also be used to study traveling modes [5], dynamics in complex structures, as shown for magnetic nanotubes [31], or (by also varying the microwave frequency) to obtain the full field-frequency-dependent microwave absorption of a given sample.

2) Nonlinear ferromagnetic resonance

As a second example, we employ the method to qualitatively study weakly nonlinear dynamics, *i.e.* the nonlinear ferromagnetic resonance. As first observed in [33], [34] and described in [35], magnetic resonances become unstable above a certain amplitude of the microwave field $\boldsymbol{h}_\mathrm{RF}$. Such phenomena are historically referred to as Suhl instabilities and are typically related to three- or four-wave scattering processes. They result in a RF-power-dependent nonlinear shift of the resonance frequencies, a line width broadening and, ultimately, in a fold-over of the absorption curves. This example is a perturbative extension of the earlier analysis-showcase towards large driving amplitudes. Strictly speaking, the Polder susceptibility has been introduced for the linear regime. At very large driving powers *e.g.* higher-harmonic contributions may appear and oscillations in the dynamical component parallel to the static external field have to be taken into account. However, at intermediate powers in the nonlinear dynamic equilibrium, the oscillations remain often well-described as being proportional to $\exp(-i\omega_\mathrm{NL}t)$ (with ω_NL being power-dependent) and the same arguments as in Sec. III can be made in an approximate manner to derive the microwave absorption.

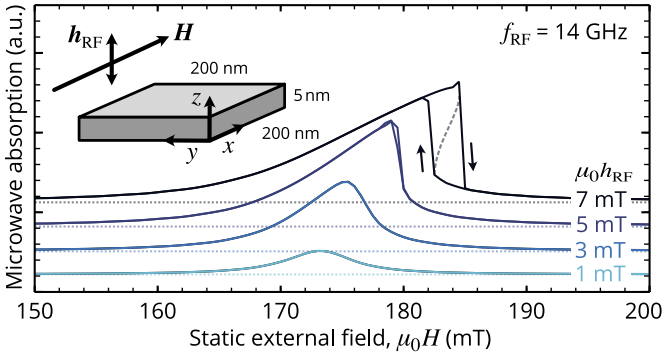

Fig. 4. Micromagnetic simulation of the field dependent FMR of a $200\,\mathrm{nm}\times200\,\mathrm{nm}\times5\,\mathrm{nm}$ element made of permalloy for different amplitudes of the RF field. For better visualization, the curves are plotted with individual baselines (dotted). For the largest amplitude a nonlinear fold-over and hysteresis in the FMR when sweeping the static field in opposite directions (arrows) is seen. A dashed curve schematically indicates the theoretical shape of the fold-over.

To showcase this, we consider a $200\,\mathrm{nm}\times200\,\mathrm{nm}\times5\,\mathrm{nm}$ element made of permalloy with exchange constant $A_\mathrm{ex} = 13\,\mathrm{pJ\,m^{-1}}$, saturation magnetization $M_\mathrm{s} = 810\,\mathrm{kA\,m^{-1}}$, reduced gyromagnetic ratio $\gamma/2\pi = 29.81\,\mathrm{GHz\,T^{-1}}$ and Gilbert-damping parameter $\alpha = 0.007$. Fig. 4 shows the numerical absorption curves for different amplitudes of the RF field. As expected for thin in-plane magnetized elements [36], we observe a positive nonlinear shift of the resonance field and a fold-over which leads to a region of bistability, *i.e.* a hysteresis in the absorption curves. Hence, the curves are shown for decreasing and increasing static external field. Note,

that the simulation of a field-step takes only half a minute (using MuMax^3 on a TITAN Xp GPU) and can be readily parallelized. A direct comparison with experimental data is cumbersome in this case and would go beyond the scope of this paper, as it requires sufficient knowledge of the microwave power arriving at the microwave antenna at hand. Note that this method can also be extended to parallel-pumping FMR [37].

V. Conclusion

We presented a numerical method to calculate FMR spectra using micromagnetic simulations. The method uses a single-frequency continuous-wave magnetic field for excitation, which allows to study the steady-state equilibrium and extract the full field-dependent dynamical susceptibility in a straight-forward manner. In contrast to common pulsed schemes, our method yields line widths and relative intensities of SWR directly comparable to those measured in FMR experiments. This eases the direct cross-identification of observed resonances, in particular for complex scenarios of nano-sized magnetic elements. The steady-state FMR spectra and magnetic excitations are directly visualized based on the default outputs of common micromagnetic codes, which renders this method easy-to-use, efficient and robust in post-processing. In addition, we showed that the nonlinear magnetic response for large driving amplitudes, such as the nonlinear frequency shift of the resonance fields or the fold-over of the absorption curves, can be studied.

This method may further be extended to analyze the transient phase prior to a dynamic equilibrium and standing wave formation processes. Such dynamic processes may become of particular interest for magnetic samples in which simple standing spin-wave formation is modified by chiral symmetry breaking and interpretation of FMR spectra requires the aid of accurate modelling. We believe, that with the recent development of high-performance micromagnetic codes, the presented method can be used as a powerful numerical method to corroborate FMR experiments and help interpret the experimentally obtained results.

Acknowledgments

We acknowledge financial support by the Deutsche Forschungsgemeinschaft (SFB 491, KA 5069/1-1, KA 5069/3-1, Project-ID 405553726 – TRR 270) as well as C. Hassel and R. Meckenstock for fruitful discussions and help in the initial stages of work. M.F. thanks for support through the Research Grant No. 075-15-2019-1886 from the Government of the Russian Federation.

References

[1] V. V. Kruglyak, S. O. Demokritov and D. Grundler, J. Phys. D: Appl. Phys. **43**, 264001 (2010)
[2] B. Lenk, H. Ulrichs, F. Garbs and M. Münzenberg, Physics Reports **507**, 107-136 (2011)
[3] M. Madami, S. Bonetti, G. Consolo, S. Tacchi, G. Carlotti, G. Gubbiotti, F. B. Mancoff, M. A. Yar and J. Åkerman, Nature Nanotechnology **6**, 635-638 (2011)
[4] G. E. W. Bauer, E. Saitoh, B. J. van Wees, Nature Materials **11**, 391-399 (2012)
[5] S. Pile, T. Feggeler, T. Schaffers, R. Meckenstock, M. Buchner, D. Spoddig, B. Zingsem, V. Ney, M. Farle, H. Wende, H. Ohldag, A. Ney, and K. Ollefs, Applied Physics Letters **116**, 072401 (2020)
[6] M.Farle, T. Silva and G. Woltersdorf, eds H. Zabel and M. Farle, Springer Tracts in Modern Physics **246**, 437 (2013)
[7] J. Lindner and M. Farle, Springer Tracts in Modern Physics **227**, 45-96 (2008)
[8] R. D. McMichael and B. B. Maranville, Phys. Rev. B **74**, 024424 (2006)
[9] G. Venkat, D. Kumar, M. Franchin, O. Dmytriiev, M. Mruczkiewicz, H. Fangohr, A. Barman, M. Krawczyk and A. Prabhakar, Magnetics, IEEE Transactions on **49**, 524-529 (2013)
[10] A. G. Gurevich and G. A. Melkov, (1996). Magnetization oscillations and waves. Retrieved from https://www.crcpress.com/Magnetization-Oscillations-and-Waves/Gurevich-Melkov/p/book/9780849394607
[11] S. V. Vonsovskij, Ferromagnetic Resonance, Pergamon Press, (1966)
[12] Code and documentation available at: http://math.nist.gov/oommf/
[13] M. J. Donahue and D. G. Porter, OOMMF user's guide, version 1.2a3, National Institute of Standards and Technology, Gaithersburg, Md, USA, 2010
[14] A. Banholzer, R. Narkowicz, C. Hassel, R. Meckenstock, S. Stienen, O. Posth, D. Suter, M. Farle and J. Lindner, Nanotechnology **22**, 295713 (2011)
[15] C. Schöppner, K. Wagner, S. Stienen, R. Meckenstock, M. Farle, R. Narkowicz, D.Suter, J. Lindner J. Appl. Phys. **116**, 033913 (2014)
[16] M. Körner, K. Lenz, A. Gallardo, M. Fritzsche, A. Mücklich, S. Facsko, J. Lindner, P. Landeros, J. Fassbender, Phys. Rev. B **88**, 054405 (2013)
[17] T. Schaffers, R. Meckenstock, D. Spoddig, T. Feggeler, K. Ollefs, C. Schöppner, S. Bonetti, H. Ohldag, M. Farle, A. Ney, Rev. Sci. Instrum. **88**, 093703 (2017)
[18] Z. Duan, C. T. Boone, X. Cheng, I. N. Krivorotov, N. Reckers, S. Stienen, M. Farle, and J. Lindner, Phys. Rev. B **90**, 024427 (2014)
[19] C. Kittel, Phys. Rev. **73**, 155-161 (1948)
[20] L. Landau and E. Lifshits, Phys. Zeitsch. der Sow. **8**, 153-169 (1935)
[21] S. V. Vonsovskij, Ferromagnetic Resonance, Pergamon Press, (1966)
[22] C. P. Poole, Electron Spin Resonance, John Wiley & Sons, (1983)
[23] B. Hillebrands, Spin Dynamics in Confined Magnetic Structures, Springer, (2002)
[24] K. Yu. Guslienko, S. O. Demokritov, B. Hillebrands and A. N. Slavin, Phys. Rev. B **66**, 132402 (2002)
[25] A. Vansteenkiste, J. Leliaert, M. Dvornik, M. Helsen, F. Garcia-Sanchez, and B. Van Waeyenberge, The design and verification of MuMax3, AIP Advances **4**, 107133 (2014).
[26] https://www.hzdr.de/db/Cms?pOid=55944pNid=107
[27] A. Kákay, E. Westphal, and R. Hertel, Speedup of FEM micromagnetic simulations with graphical processing units, IEEE Transactions on Magnetics **46**, 2303 (2010).
[28] https://fangohr.github.io/research/micromag.html
[29] M. R. Scheinfein, LLG Micromagnetics Simulator, Software for Micro-Magnetic Simulations, see http://llgmicro.home.mindspring.com/ (1997).
[30] Banholzer, A., Narkowicz, R., Hassel, C., Meckenstock, R., Stienen, S., Posth, O., Stuter, D., Farle, M., Lindner, J. (2011). Visualization of spin dynamics in single nanosized magnetic elements, https://doi.org/10.1088/0957-4484/22/29/295713
[31] Lenz, K., Narkowicz, R., Wagner, K., Reiche, C. F., Körner, J., Schneider, T., Kákay, A., Schultheiss, H., Weissker, U., Wolf, D., Suter, D., Büchner, B., Fassbender, J., Mühl, T., Lindner, J. (2019). Small, 15(49), 1904315. https://doi.org/10.1002/smll.201904315
[32] Cansever, H., Narkowicz, R., Lenz, K., Fowley, C., Ramasubramanian, L., Yildirim, O., Niesen, A.,Huebner, T., Reiss, G., Lindner, J., Fassbender, J., Deac, A. M. (2018). J. Phys. D: Appl. Phys, 51, 224009–224019. https://doi.org/10.1088/1361-6463/aac03d
[33] N. Bloembergen, R. W. Damon, Physical Review, 85(4), 699–699. (1952) https://doi.org/10.1103/PhysRev.85.699
[34] Damon, R. W. (1953). Reviews of Modern Physics, 25(1), 239–245. https://doi.org/10.1103/RevModPhys.25.239
[35] Suhl, H. (1957). The theory of ferromagnetic resonance at high signal powers. Journal of Physics and Chemistry of Solids, 1(4), 209–227. https://doi.org/10.1016/0022-3697(57)90010-0
[36] Krivosik, P., Patton, C. E. (2010). Hamiltonian formulation of nonlinear spin-wave dynamics: Theory and applications. Physical Review B, 82(18), 184428. https://doi.org/10.1103/PhysRevB.82.184428
[37] Venugopal, A., Qu, T., Victora, R. H. (2020). Nonlinear Parallel-Pumped FMR: Three and Four Magnon Processes. IEEE Transactions on Microwave Theory and Techniques, 68(2), 602–610. https://doi.org/10.1109/TMTT.2019.2952128